Available online at www.sciencedirect.com

ScienceDirect

Geochimica et Cosmochimica Acta 317 (2022) 138–154

Geochimica et Cosmochimica Acta

www.elsevier.com/locate/gca

Stable chromium isotopic variations in peridotite mantle xenoliths: Metasomatism versus partial melting

M. Jerram [a,b,*], P. Bonnand [c], J. Harvey [d], D. Ionov [e], A.N. Halliday [b]

[a] Department of Earth Sciences, University of Oxford, Oxford, OX1 3AN, UK
[b] Lamont-Doherty Earth Observatory, Columbia University, Palisades, NY 10964, USA
[c] Univ. Brest, CNRS, Laboratorie Geosciences Ocean, UMR6538, IUEM, 29280, Plouzane, France
[d] School of Earth and Environment, University of Leeds, Leeds LS2 9JT, UK
[e] Geosciences Montpellier, Université de Montpellier, 34095 Montpellier, France

Received 26 February 2021; accepted in revised form 22 October 2021; available online 29 October 2021

Abstract

Chromium isotope compositions have been determined for 42 mantle-derived xenoliths from Cameroon, France, Mongolia, Russia and the USA. The samples are mainly spinel and garnet lherzolites, or harzburgites, and yield $\delta^{53}Cr_{NIST979}$ from −0.33 to 0.43‰, within the range of previously reported compositions, −0.51 to 0.74‰ (Xia et al., 2017). Partial melting has been proposed as a process that alters the $\delta^{53}Cr$ of the mantle residue. New non-modal melting models show that the compatible nature of Cr is inconsistent with large changes in the residue's isotopic composition. The fractionation during melting is constrained by calculated $\Delta^{53}Cr_{mantle\text{-}melt}$-values <0.09 and the measured $\Delta^{53/52}Cr$ mantle-melt ≈ 0.07‰, which is too small to generate the observed range in $\delta^{53}Cr$ at low to medium degrees of melting. Fertile to melt-depleted, unmetasomatised peridotite xenoliths show no correlations between $\delta^{53}Cr$ and indicators of partial melting. Almost all LREE-enriched samples studied here define a correlation between $\delta^{53}Cr$ and $(La/Yb)_N$. This is consistent with alteration of Cr isotopic compositions by some process that is related to interactions with low degree partial melts. The low Cr content of small degree partial melts renders metasomatism via such liquids a difficult explanation for the isotopic effects found. A possible explanation is some form of disequilibrium loss of isotopically light Cr into such liquids during their percolation through the mantle. This is similar to a previously proposed mechanism of kinetic isotopic fractionation of Cr associated with interactions between silicate melts and peridotitic mantle (Xia et al., 2017).

© 2021 The Authors. Published by Elsevier Ltd. This is an open access article under the CC BY-NC-ND license (http://creativecommons.org/licenses/by-nc-nd/4.0/).

Keywords: Cr isotopes; Mantle; Partial melting; Metasomatism

1. INTRODUCTION

Transition metal isotope compositions can be fractionated at high temperatures, depending on, for example, oxidation states, mineral phases, disequilibrium exchange and volatilisation (Schauble, 2004). It now is possible to resolve and utilize such small mass fractionations in chromium (Cr) isotope compositions as a diagnostic tool for such processes (Schoenberg et al., 2008). For example, loss of moderately volatile Cr may explain the light isotopic compositions found in Vesta and the Moon (Sossi et al., 2018; Zhu et al., 2019).

A key issue of interest has been whether Cr isotopes could be used to interrogate core formation. The behaviour of Cr during metal-silicate separation depends upon the oxygen fugacity of the body, as well as temperature and pressure (Wade and Wood, 2005; Wood et al., 2008;

* Corresponding author at: Lamont-Doherty Earth Observatory, Columbia University, Palisades, NY 10964, USA
E-mail address: mj2964@columnbia.edu (M. Jerram).

https://doi.org/10.1016/j.gca.2021.10.022
0016-7037/© 2021 The Authors. Published by Elsevier Ltd.
This is an open access article under the CC BY-NC-ND license (http://creativecommons.org/licenses/by-nc-nd/4.0/).

Siebert et al., 2011). Chromium isotope variations are expressed as $\delta^{53}Cr$, the $^{53}Cr/^{52}Cr$ ratio normalised to that of the National Institute of Standards and Technology, Standard Reference Material (SRM) 979 in parts per mil (Ellis et al., 2002). Large fractionations have been discovered in iron meteorites resulting from the fractional crystallisation of protoplanetary core material (Bonnand & Halliday, 2018). In contrast, the isotopic composition of the bulk silicate Earth (BSE) is similar to all classes of chondrites (Bonnand et al., 2016; Schoenberg et al., 2016), which implies little fractionation during silicate-metal segregation. This can be reconciled with Cr isotope fractionation factors calculated in Moynier et al. (2011), for the special case on Earth, where Cr is more siderophile at the especially high temperatures and pressures of partitioning (Drake et al., 1989).

To ascertain the precise degree of isotopic fractionation during core formation requires determination of the exact $\delta^{53}Cr$ of the BSE. Mantle peridotites display considerable $\delta^{53}Cr$ heterogeneity, leading to large uncertainties in BSE estimates (Schoenberg et al., 2008; Xia et al., 2017). Although this problem has been circumvented by using mantle derived chromites (Farkaš et al., 2013), and komatiites that sample larger volumes of the mantle (Sossi et al., 2018; Jerram et al., 2020; Wagner et al., 2021), the exact causes of mantle variability in Cr isotope composition have not been determined.

The behaviour of Cr during melting depends on the oxidation state. Chromium occurs as Cr^{2+} and Cr^{3+} in the mantle. Higher temperatures, lower oxygen fugacity will increase Cr^{2+}/Cr_{TOT} ($Cr_{TOT} = Cr^{2+}+Cr^{3+}$; Schreiber & Haskin, 1976; Li et al., 1995; Berry et al., 2006). The composition of melts can also affect the Cr^{2+}/Cr_{TOT}, e.g., strongly basic melts stabilise lower Cr^{2+}/Cr_{TOT} (O'Neill and Berry, 2021). The modern mantle is relatively oxidised, which means that Cr^{3+} is prevalent (Berry et al., 2006). Trivalent Cr is largely compatible in the octahedral sites of pyroxenes, garnets and spinels, which produces low Cr melts. While the Cr concentration in mantle peridotites is variable (Liang & Elthon, 1990; Ionov & Hofmann, 2007), it does not correlate with degree of melt extraction. This has been explained by mantle peridotites retaining a signature of ancient melt extraction at higher temperatures and degrees of melting (Liang and Elthon, 1990); conditions where Cr would be less compatible (Li et al., 1995).

Two explanations for the $\delta^{53}Cr$ variations in mantle peridotites have been proposed, melt-rock interactions (metasomatism) and partial melting (Xia et al., 2017; Shen et al., 2018). The extent to which these processes affect mantle peridotites is unresolved, leading to uncertainty in the interpretation of $\delta^{53}Cr$ variations. An initial study by Schoenberg et al. (2008) found no resolvable difference between the Cr isotope composition of the mantle and that of partial melts, and concluded that Cr isotopes do not fractionate during melting. However, Xia et al. (2017) argued that, while the variability in $\delta^{53}Cr$ of mantle peridotites cannot be explained by melting alone, it can produce variations of up to $\delta^{53}Cr = 0.2‰$. Isotopic fractionation factors (α-values where $\ln(\alpha) \approx \Delta^{53}Cr_{residue\text{-}melt}$) for melting ranging from 1.0002 to 1.0008 were given, based on the identification of a trend between $\delta^{53}Cr$ and Al_2O_3 (wt.%) (Xia et al., 2017). Later studies found that partial melts formed with $\delta^{53}Cr$ values that are only 0–0.07‰ ($\alpha = 1.00000$–1.00007) lower than the mantle (Sossi et al., 2018; Bonnand et al., 2020a,b; Jerram et al., 2020; Shen et al., 2020), which agrees with experiments from Berry et al. (2021a,b) Therefore, the relative contributions of partial melting and post-melting processes to the large heterogeneity observed in xenoliths is unresolved.

Kinetic fractionation during melt percolation and metasomatism have been proposed as other processes that can provide much greater $\delta^{53}Cr$ variations in mantle peridotites. Xia et al. (2017) reported contrasting Cr isotope compositions in pyroxenite veins and their host peridotites. The authors argued that chromatographic interactions lead to a transfer of kinetically fractionated isotopically light Cr from mantle peridotites into silicate melts. Isotopically heavy and light $\delta^{53}Cr$ compositions of mantle peridotites can be created across the gradient of this chromatographic model. Variations of $\delta^{53}Cr$ in mantle peridotites produced by metasomatism were also identified by Shen et al., (2018), who suggested that they could be due to mineral-melt interactions and/or kinetic diffusion. Ionic models can be used to estimate the chromium isotopic composition of minerals in equilibrium, which should yield $\delta^{53}Cr$ of spinel > clinopyroxene = orthopyroxene > olivine (Shen et al., 2018). However, mineral separates do not always display this trend (Xia et al., 2017; Shen et al., 2018; Supplementary Information) providing evidence they may not always be in equilibrium, possibly because of metasomatism.

This study expands on previous work and reports high precision Cr isotope measurements of a large set of well-characterised mantle peridotites, allowing interrogation of partial melting effects. The samples are from four continents, representing a range of lithologies and compositions. We also reassess published melting models and introduce new non-modal melting equations. Using these more appropriate and internally consistent models, the limits on $\delta^{53}Cr$ variation from melting of mantle peridotites can be quantified and shown to be very small. Geochemical data are used to provide evidence that other processes, probably metasomatic, are mainly responsible for changes in mantle $\delta^{53}Cr$.

2. SAMPLES

Forty-one peridotite xenoliths and one pyroxenite were selected for this study. The classification of ultramafic xenoliths in this study follows that of Streckeisen (1976). The peridotites were chosen to provide an overview of typical rocks in the mantle lithosphere. To avoid the effects of low temperature alteration, fresh, un-weathered samples were selected. The peridotites show a broad range in the amount of melt extraction, and some display petrological and geochemical indicators of metasomatism.

This study includes fertile and unmetasomatised peridotites from Tariat, Mongolia and Vitim, Siberia which have compositions approaching that of the BSE (Fig. 1; Preβ et al., 1986; Ionov et al., 1993a,b; Ionov, 2007). The

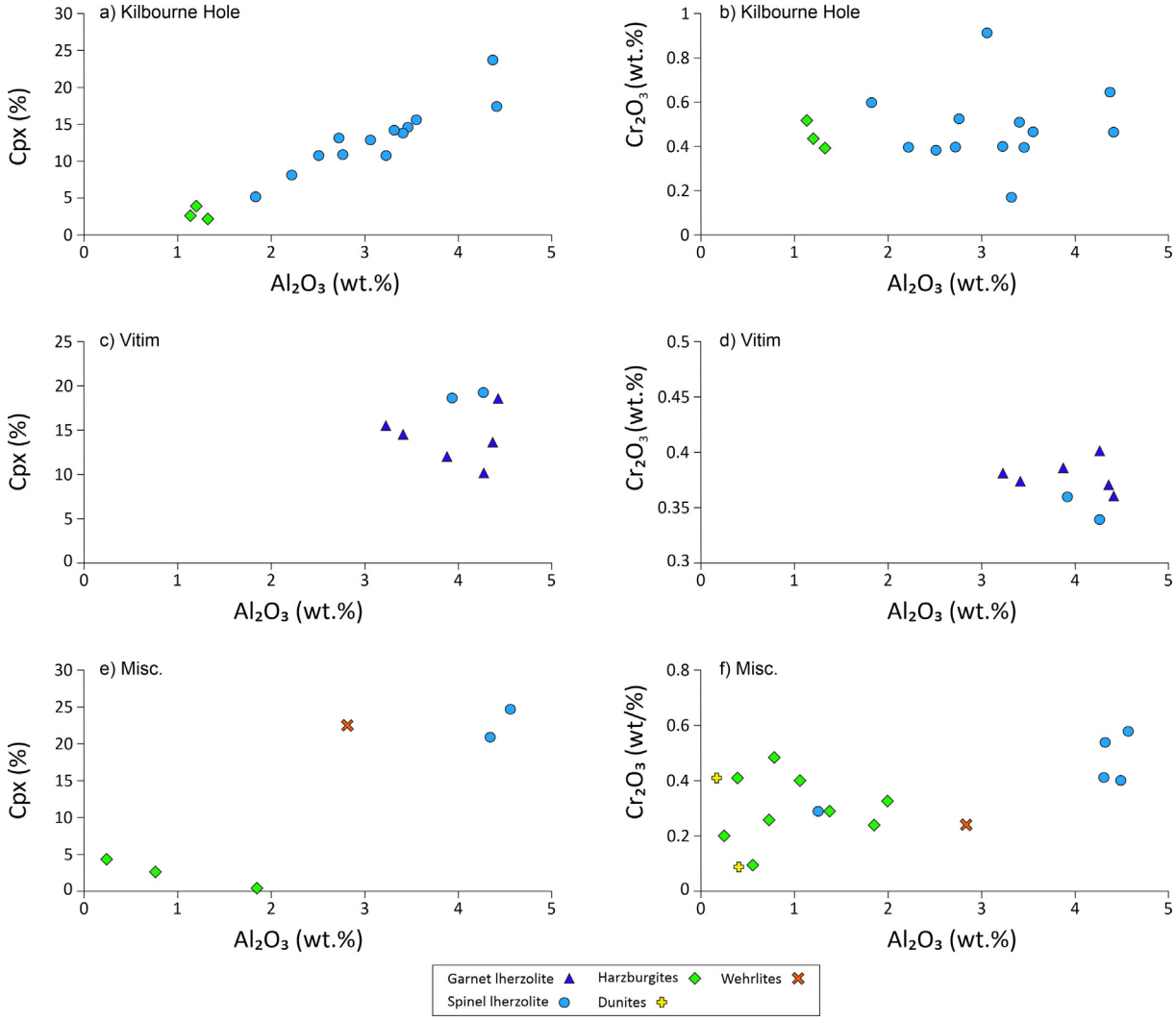


Fig. 1. Al_2O_3 (wt.%) versus modal abundance of clinopyroxene (cpx) and Cr_2O_3 (wt.%) for mantle peridotites in this study. The Kilbourne Hole and Vitim suites of peridotites are presented separately from other samples. The samples from Kilbourne Hole show a strong correlation between cpx and Al_2O_3 (wt.%) reflecting the influence of melting, while the Vitim samples have little variation and are close to the composition of the BSE (Preβ et al., 1986; Ionov et al., 1993a,b; Ionov, 2007). The other samples show a general positive trend between cpx and Al_2O_3 (wt.%). No variations between Cr_2O_3 (wt.%) and Al_2O_3 (wt.%) are seen for any of the suites, in agreement with previous studies (Liang and Elthon, 1990).

peridotites from Kilbourne Hole, New Mexico included in this study exhibit the effects of variable melting (Fig. 1), metasomatism, melt-rock refertilisation (KH03-3 and KH96-8) as well as interactions between the xenoliths and their host magma, which has led to spongy clinopyroxene KH03-10, KH03-15, KH03-24 and KH03-27), and interstitial glass (KH03-15, KH03-16 and KH03-21; Harvey et al., 2011, 2012, 2015). Interactions with melts and fluids that took place in the mantle before entrapment in the host magma have been recorded in other samples, including enrichment in FeO by percolating melts of samples 8530-24 and 8531-40; and infiltration of a Ca- and Fe rich melt of Tok 10-1, which enriched the Fe isotope composition by $\delta^{56}Fe = +0.06‰$ (Weyer and Ionov, 2007).

The suite of samples measured in this study show correlations between different indicators of partial melting (Al_2O_3 wt.%, CaO wt.%, cpx % and Mg#; Fig. S5), however, there is no correlation between these indicators of partial melting and Cr concentration (Fig. 1), consistent with the findings of Liang & Elthon, (1990). All samples have previously been studied and are well characterised in the literature (e.g. Reid et al., 1975; Rhodes & Dawson, 1975; Lee et al., 1996; Ionov, 2004; Ionov et al., 2006; Williams et al., 2005; Weyer & Ionov, 2007; Pogge von Strandmann et al., 2011; Gibson et al., 2013; Harvey et al., 2011, 2012, 2015; Prytulak et al., 2013).

2.1. Lherzolites

Twenty-seven lherzolites were included in this study. These are from Kilbourne Hole, New Mexico (n = 13); Vitim, Siberia (n = 8); Tariat, Mongolia (n = 2);

Ngaoundéré, Cameroon (n = 2); Labait Hills, Tanzania (n = 1); Massif Central, France (n = 1). The Cr_2O_3 concentrations range from 0.15 to 0.92 wt.%. The Al_2O_3 concentrations are from 1.8 to 4.6 wt.%. The bulk Mg# (Mg/(Mg + Fe)) varies from 0.89-0.92. The lherzolites in this study are both spinel and garnet bearing (Table 1). The garnet lherzolites have spinel, olivine and pyroxene inclusions in the garnet (Ionov et al., 2005a,b).

2.2. Harzburgites

Eleven harzburgites were selected for this study. These are from Tariat, Mongolia (n = 4); Kilbourne Hole, USA (n = 3); Lashaine, Tanzania (n = 2); Kamchatka, Russia (n = 1); Dariganga, Mongolia (n = 1). Harzburgites have lower abundances of the moderately incompatible elements, (Ca, Al, Na). The compositions of these harzburgites are more melt-depleted, with higher Mg# (0.9–0.93) and lower Al_2O_3 (0.72 to 2.00 wt.%) than lherzolites. The Cr_2O_3 concentrations range from 0.09 to 0.49 wt.%.

2.3. Dunites

Two dunites were measured in this study, both of which came from Lashaine, Tanzania. They have Cr_2O_3 of 0.09 and 0.41 wt.% and are highly depleted in Al_2O_3 (0.16 and 0.4 wt.%). Dunites are thought to form either by the accumulation of crystallising olivine in melt channels, during extremely high degrees of partial melting, or through replacement of pyroxene by olivine (Kelemen et al., 1995, 1997; Gibson et al., 2013).

2.4. Wehrlites

One wehrlite from Tok, SE margin of the Siberian craton, was measured in this study (Tok 10-1). This sample has a Cr_2O_3 of 0.25 wt.% and Al_2O_3 of 2.8 wt.%. This sample belongs to a lherzolite-wehrlite trend created by infiltration of an Fe- and Ca-rich, Si undersaturated melt, which replaced orthopyroxene by clinopyroxene and increased the FeO and CaO concentrations to 11.8 wt.% and 4.6 wt.% respectively. Wehrlites are believed to have formed through refertilisation of the mantle, usually through interactions with silicate melts (Ionov et al., 2005a,b).

2.5. Pyroxenites

Pyroxenites have more than 60 % pyroxene (Streckeisen, 1976) and can be formed from trapped melts, melt-rock interactions or recycled material (Davies et al., 1993; Santos et al., 2002; Downes, 2007). The pyroxenite measured in this study, P6, is from Ngaoundéré, Cameroon, which is believed to have formed as a trapped melt (Lee et al., 1996). It has a Cr_2O_3 content of 0.15 wt.% and Al_2O_3 of 13.3 wt.% (Lee et al., 1996).

3. ANALYTICAL METHODS

Measurements of Cr isotopic mass dependent fractionation followed the method previously published by (Bonnand et al., 2016). A summary is provided here. All acids were purified by in-house sub-boiling distillation. Dissolutions were first carried out on hotplates, while samples with refractory material were also dissolved using high-pressure Parr bombs. Hotplate dissolutions first used a HNO_3 and HF mixture followed by drying down and redissolving in 6 M HCl. Parr bomb dissolutions utilised 6 M HCl at 200 °C. If undissolved material remained, samples were dried, and fresh acid added before repeating the dissolution.

Mass fractionation occurring during chemical separation and isotopic measurement (mass bias) were corrected using the double spike method (e.g. Albaréde & Beard, 2004). Samples were spiked with a ^{50}Cr - ^{54}Cr double spike, prior to Cr purification, and left to equilibrate on hotplates. The Cr separation follows the method developed in (Bonnand et al., 2016). Two AG 50 W-X8 cation exchange resin columns were deployed: the first removed matrix elements, and the second specific isobaric interferences (^{50}Ti, ^{50}V and ^{54}Fe). Chromium blanks were negligible (<4 ng) compared to the total amount processed (2 μg).

Samples were measured on a ThermoScientific Triton thermal ionisation mass spectrometer (TIMS) in static multicollection mode at the University of Oxford. Samples were loaded onto an outgassed Re filament, together with silica gel and a boric acid activator. Each measurement consisted of 54 blocks of 10 cycles, each cycle lasting 8.4 seconds, with a baseline of 50 seconds measured after every block. High precision measurements using TIMS was possible due to the long-term stability of the ion beam. Along with the Cr isotopes (50, 52, 53 and 54), masses 49, 51 and 56 were monitored and used to correct isobaric interferences from Ti, V and Fe respectively. An amplifier gain calibration was performed daily. Amplifier rotations were carried out through the run. The double spike deconvolution was performed offline using an iterative procedure following that of Bonnand et al., (2011).

The 2 standard error internal precision for each run was typically less than 0.01‰. Uncertainty of the measurements was assessed by repeat measurements of JP-1 over a three-year period, yielding $\delta^{53}Cr = -0.108 \pm 0.019$‰ (2 s.d., n = 11), which closely matches previous measurements of the standard, and defines an intermediate precision comparable to that of previous work (Schoenberg et al., 2008; Bonnand et al., 2016; Xia et al., 2017; Bonnand et al., 2020a,b).

4. RESULTS

The $\delta^{53}Cr$ values for peridotites are presented in Table 1 and Fig. 2. Data for separated constituent mineral phases are presented in the Supplementary Information and Fig. 3. The mantle peridotites display $\delta^{53}Cr$ values from −0.33 to +0.43‰, within the range of published data ($\delta^{53}Cr = -0.51$ to +0.74‰; Schoenberg et al., 2008; Xia et al., 2017). Mantle peridotites measured in this study are more variable than mafic and ultramafic magmatic rocks ($\delta^{53}Cr = -0.21$ to −0.01‰; Schoenberg et al., 2008; Sossi et al., 2018; Shen et al., 2020; Bonnand et al., 2020a,b; Jerram et al., 2020) and diverge considerably from

Table 1
Table showing the bulk rock geochemical data for Cr, Al_2O_3, #Mg and $(La/Yb)_N$ (normalised to the primitive mantle (Palme and O'Neill, 2014)). Concentrations are taken from the literature (Reid et al., 1975; Rhodes & Dawson, 1975; Lee et al., 1996; Ionov, 2004; Ionov et al., 2006; Weyer & Ionov, 2007; Harvey et al., 2012; Gibson et al., 2013) or were measured in house using the Thermo Finnigan Element 2 at the Department of Earth Sciences, Oxford. Additional geochemical and petrological data on these samples are provided in the Supplementary Information. [a] chromium concentrations determined using isotope dilution.

Sample	Rock Descriptor	Location	Cr ($\mu g.g^{-1}$)	$\delta^{53}Cr$	2 s.e.	Al_2O_3 (wt%)	Mg#	$(La/Yb)_N$
Vi313-1	Gr Lhz	Vitim, Russia	2531	−0.17	0.006	4.4	0.895	0.90
Vi313-6	Gr Lhz	Vitim, Russia	2599	−0.11	0.006	3.9	0.893	0.89
Vi313-102	Gr Lhz	Vitim, Russia	2462	−0.14	0.007	4.5	0.890	0.88
Vi313-104	Gr Lhz	Vitim, Russia	2551	−0.11	0.005	3.7	0.892	0.89
Vi313-106	Gr Lhz	Vitim, Russia	2736	−0.08	0.008	3.3	0.895	0.89
Vi313-112	Gr Lhz	Vitim, Russia	2633	−0.11	0.005	4.2	0.894	0.89
Vi314-56	Sp Lhz	Vitim, Russia	2326	−0.19	0.025	4.3	0.888	0.89
Vi314-58	Sp Lhz	Vitim, Russia	2462	−0.15	0.009	3.9	0.893	0.90
Mo-101	Sp Lhz	Tariat, Mongolia	2804	−0.09	0.005	4.3	0.910	0.46
MOG-1	Sp Lhz	Tariat, Mongolia	2736	−0.12	0.004	4.5	0.890	3.26
PB-XEN1	Sp Lhz	Central Massif, France	n.d.	−0.13	0.014	n.d.	n.d.	2.35
KH03.02	Sp Lhz	Kilbourne Hole, USA	2051[a]	−0.17	0.004	2.8	0.916	0.54
KH03.03	Sp Lhz	Kilbourne Hole, USA	2535[a]	−0.17	0.007	4.4	0.903	0.40
KH03.6	Sp Lhz	Kilbourne Hole, USA	1765[a]	−0.22	0.003	3.3	0.914	0.34
KH03.7	Sp Lhz	Kilbourne Hole, USA	1496[a]	0.01	0.007	2.5	0.916	0.34
KH03.10	Sp Lhz	Kilbourne Hole, USA	1557[a]	−0.32	0.006	3.2	0.912	1.39
KH03.11	Sp Lhz	Kilbourne Hole, USA	2074[a]	0.00	0.005	3.6	0.909	0.25
KH03.18	Sp Lhz	Kilbourne Hole, USA	1990[a]	−0.09	0.003	3.4	0.911	0.14
KH03.21	Sp Lhz	Kilbourne Hole, USA	1812[a]	−0.10	0.004	4.4	0.903	0.31
KH03.24	Sp Lhz	Kilbourne Hole, USA	1551[a]	0.40	0.005	2.7	0.904	0.74
KH03.25	Sp Lhz	Kilbourne Hole, USA	2709[a]	0.07	0.007	2.2	0.919	0.19
KH96.2	Sp Lhz	Kilbourne Hole, USA	2336[a]	−0.11	0.007	1.8	0.923	0.22
KH96.8	Sp Lhz	Kilbourne Hole, USA	3575[a]	−0.17	0.003	3.1	0.917	1.81
KH96.18	Sp Lhz	Kilbourne Hole, USA	1549[a]	−0.10	0.005	3.5	0.908	0.03
C235D	Sp Lhz	Mt Cameroon	3984	−0.08	0.006	4.6	n.d.	n.d.
H93-X8	Sp Lhz	Laibat Hill, Tanzania	2051	−0.08	0.020	n.d.	n.d.	n.d.
P13	Sp Lhz	Ngaoundere, Cameroon	3700	−0.15	0.005	4.3	n.d.	n.d.
4500-18	Sp Hzb	Tariat, Mongolia	1778	−0.12	0.006	0.7	0.927	61.71
4500-19d	Sp Hzb	Tariat, Mongolia	2736	−0.02	0.006	1.1	0.923	6.92
8530-24	Sp Hzb	Tariat, Mongolia	2257	0.43	0.003	2.0	0.899	12.95
8531-40	Sp Hzb	Tariat, Mongolia	1984	0.39	0.007	1.2	0.900	8.70
BN-8	Sp Hzb	Dariganga, Mongolia	2017	−0.14	0.004	1.3	0.919	n.d.
Av-8	Sp Hzb	Kamchatka, Russia	3333	−0.14	0.005	0.8	0.911	1.43
KH03.15	Sp Hzb	Kilbourne Hole, USA	1701[a]	−0.10	0.007	1.2	0.919	1.96
KH03.16	Sp Hzb	Kilbourne Hole, USA	2302[a]	−0.02	0.004	1.1	0.926	4.74
KH03.27	Sp Hzb	Kilbourne Hole, USA	2168[a]	−0.25	0.010	1.3	0.922	0.34
BD-774	Sp Hzb	Lashaine, Tanzania	1368	0.03	0.005	0.2	0.920	n.d.
BD-822	Sp Hzb	Lashaine, Tanzania	1642	−0.06	0.007	1.9	0.930	n.d.
BD-806	Dunite	Lashaine, Tanzania	616	−0.33	0.044	0.4	0.808	n.d.
BD-825	Dunite	Lashaine, Tanzania	2804	−0.19	0.057	0.2	n.d.	n.d.
Tok-10-1	Wehrlite	Tokinsky, Siberia	1689	−0.06	0.005	2.8	0.848	n.d.
P6	Pyroxenite	Ngaoundere, Cameroon	1014	−0.35	0.044	13.3	n.d.	n.d.
JP1	Peridotite	Geological Reference	2807	−0.11	2 s.d.	0.019		

the BSE value ($\delta^{53}Cr = -0.12 \pm 0.04‰$, Jerram et al. 2020). Although the data span a 0.76‰ range, 20 samples yield values that are within the uncertainty of the BSE ($\delta^{53}Cr = -0.12 \pm 0.04‰$).

The compositions of spinel and garnet bearing lherzolites are similar, with garnet lherzolites having a narrow range, $\delta^{53}Cr = -0.17$ to $-0.08‰$, towards the middle of the range of spinel lherzolites. The range in compositions of the lherzolites ($\delta^{53}Cr = -0.33$ to $+0.40‰$) and harzburgites ($\delta^{53}Cr = -0.25$ to $+0.43‰$) are similar. The $\delta^{53}Cr$ of dunites ranges from -0.33 to $-0.19‰$, which is only slightly lower than previously measured dunites ($\delta^{53}Cr = -0.17$ to $-0.12‰$; Schoenberg et al., 2008; Xia et al., 2017). The wehrlite ($\delta^{53}Cr = -0.06‰$) is within the range of the BSE. The pyroxenite, P6, is much lighter than the BSE ($\delta^{53}Cr = -0.35‰$) but within range of previously measured pyroxenites, $\delta^{53}Cr = -1.36$ to $-0.05‰$ (Xia et al., 2017). The $\delta^{53}Cr$ of samples measured in this study have been compared to a range of different variables, including mineral abundance, equilibrium temperature and geochemical data, which are presented in the Supplementary Information. Only significant features are discussed below.

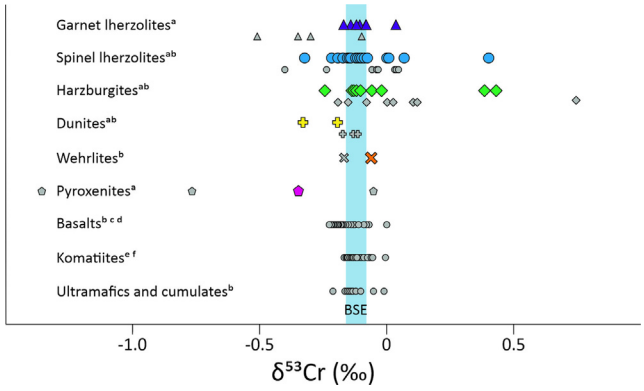


Fig. 2. Isotopic composition of Cr in mantle xenoliths and crustal samples. Data from this study is in coloured symbols, data from previous work is shown in grey symbols, a= Xia et al., 2017; b= Schoenberg et al., 2008; c= Shen et al., 2020; d = Bonnand et al., 2020a,b; e= Sossi et al., 2018; f= Jerram et al., 2020. The BSE (-0.12 ± 0.04‰) is shown with the blue bar (Jerram et al., 2020). Measurements from this study are within range of previous measurements, apart from the dunites. One of the dunites measured within this study is lighter than the range of previous Cr isotope measurements. Crustal rocks show a smaller range of value, which lies closer to the BSE.

5. DISCUSSION

5.1. Chromium isotope behaviour during partial melting

As outlined above, previous studies disagree on whether and how the Cr isotope composition of the mantle fractionates during partial melting (Schoenberg et al., 2008; Xia et al., 2017). Isotopic fractionation during melting can be estimated using the difference in composition between partial melts and the mantle. Two recent studies have provided evidence that a small fractionation ($\Delta^{53}Cr_{mantle\text{-}melt} \approx 0.07$‰) is achieved during basalt melt production (Bonnand et al., 2020a,b; Shen et al., 2020). However, the effect on the residual mantle of the generation of such melts that are only slightly isotopically fractionated is unclear. One reason for the lack of clarity is that the formulation of melting models deployed to understand isotopic fractionation may not have been appropriate. Therefore, these models are corrected in the following.

The behaviour of Cr isotopes during mantle melting can be quantified with modal and non-modal models. The former assumes that the minerals in the mantle assemblage always melt in fixed proportions according to their modal abundance in the original solid. Non-modal melting models consider the differing rates at which minerals melt using the "P-value" (Eq. (1)). The following equations use the notation, x, s and l to denote mineral, solid and liquid phases respectively. The "P-term" combines the partition coefficient ($D_{x/l}$) for Cr in each mineral with the melting reaction γ_x (Shaw, 1970). The melting reaction (γ) is normalised to the mass of liquid formed, so by definition the sum of the melting reactions over all minerals will be 1.

$$P = \sum_x (D_{x/l}\gamma_x) \tag{1}$$

Spinel and clinopyroxene (cpx) are the major Cr bearing phases in the fertile upper mantle (e.g. Woodland et al., 2006). During melting, spinel is consumed non-modally, therefore at low degrees of melting it contributes a greater fraction of the melt (0.09–0.12) than its abundance in the mantle (0.01–0.03; Gudfinnsson & Presnall, 1996). Garnet bearing peridotites mainly contain Cr in garnet and cpx, which are both exhausted during melting earlier than orthopyroxene and olivine (Baker & Stolper, 1994; Walter, 1998). Therefore, as spinel, garnet and clinopyroxene are consumed preferentially, non-modal melting models are required to describe the behaviour of Cr. The melting equations used in this study are for incongruent melting, with olivine produced at low pressures and orthopyroxene at higher pressures (Table 2).

Models to describe isotope variation have been developed in recent years, e.g. (Dauphas et al., 2009; Sossi & O'Neill, 2017; Wang et al., 2018). The models described here for Cr isotopes are modified from those presented in Shaw (1970) for element concentrations and in Sossi and O'Neill (2017) for isotope ratios. Shaw (1970) derived equations for non-modal fractional (Eqs. (2) and (3)) and batch (Eqs. (4) and (5)) melting. The output of the models is the ratio of the concentration in the accumulated liquid (C_l), batch liquid ($C_{\bar{l}}$) or residual mantle (C_r) over the initial mantle (C_0), in terms of the fraction of melting (F). These models use a constant initial bulk coefficient (D_0) and P-value.

$$\frac{C_l}{C_0} = \frac{1}{F}\left(1 - \left(1 - P\left(\frac{F}{D_0}\right)\right)^{\left(\frac{1}{P}\right)}\right) \tag{2}$$

$$\frac{C_r}{C_0} = \frac{1}{1-F}\left(1 - P\left(\frac{F}{D_0}\right)\right)^{\left(\frac{1}{P}\right)} \tag{3}$$

$$\frac{C_{\bar{l}}}{C_o} = \frac{1}{D_o + F(1-P)} \tag{4}$$

$$\frac{C_r}{C_o} = \left(\frac{D - P \times F}{1-F}\right) \times \left(\frac{1}{D_o + F(1-P)}\right) \tag{5}$$

Sossi and O'Neill (2017) showed that by treating isotopes as separate elements, Eqs. (2)–(4) could be modified to calculate the isotope ratio variations during melting. At high temperatures the approximation can be made that

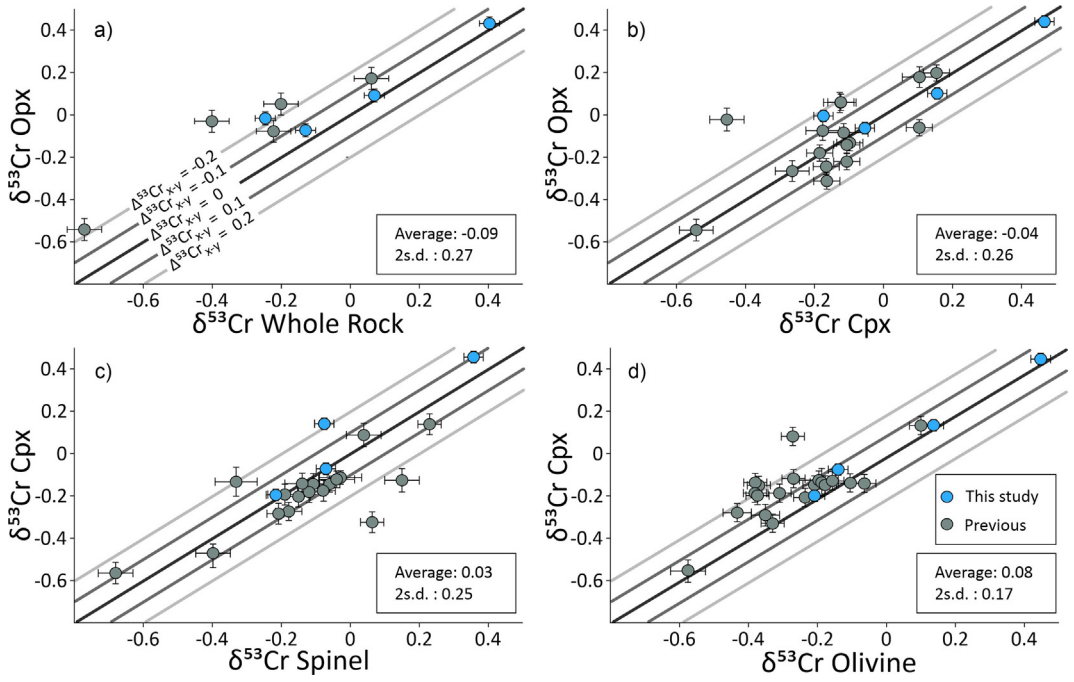


Fig. 3. δ^{53}Cr of mineral separates and whole rock compositions plotted as pairs. a) Whole Rock vs. opx; b) cpx vs. opx c) spinel vs cpx and d) olivine vs cpx. Phases are plotted as pairs to highlight the difference in composition between all data. The grey line represent the difference in composition between the phase of the x axis – the y axis. Data is taken from this study and previous studies (Xia et al., 2017; Shen et al., 2018). The average $\Delta_{x\text{-}y}$ composition and two times standard deviation is shown.

the partition coefficient of an isotope (j) is the same as the element (Eq. (6), Sossi & O'Neill, 2017). The small difference in partition coefficient between two isotopes (i and j) is proportional to the fractionation factor ($\alpha E^{i/j}_{1-2}$, where E is the element of interest; Eq. (7)).

$$D^j_{s/l} \approx \sum_x D_{x-l} \tag{6}$$

$$D^i_{s/l} = \left(\alpha E^{\frac{i}{j}}_{s/l}\right) D^j_{s/l} \tag{7}$$

The corresponding expressions for P values are derived in the same manner. At high temperatures P^j_{s-l} will be approximately the same as P (Eq. (8)). The partition coefficients used to calculate $P^i_{s/l}$ will also be proportional to $P^j_{s/l}$ through $\alpha E^{\frac{i}{j}}_{s/l}$. The fractionation factor, $\alpha E^{\frac{i}{j}}_{s/l}$, is constant over the sum of minerals, therefore, $P^i_{s/l}$ is given using the Eq. (9). Further details on the derivation of these equations can be found in Sossi and O'Neill (2017).

$$P^j_{s/l} \approx \mathrm{P} = \sum_x (D_{x/l}\gamma_i) \tag{8}$$

$$P^i_{s/l} \approx (\alpha E^{\frac{i}{j}}_{s/l}) \sum_s (D_{s/l}\gamma_s) \approx \alpha E^{\frac{i}{j}}_{s/l} * P^j_{s/l} \tag{9}$$

Eqs. (10) and (11) for fractional melting and Eqs. (12) and (13) for batch melting represent the behaviour of isotope-*i* during melting and include the terms for D and P from Eqs. (7) and (9). The behaviour of isotope-*j* is assumed to be the same as element E, therefore is modelled using Eqs. (2)–(5). In Eqs. (10) and (11), $\alpha E^{i/j}_{1-2}$ terms cancel between the bulk coefficient and one of the P-values. Eq. (14) is used to convert the isotope ratio (calculated using the concentrations of isotope-i and isotope-j) into the delta notation.

$$\frac{C^i_l}{C^i_o} = \frac{1}{F}\left(1 - \left(1 - P_j\left(\frac{F}{D^j_{s/l}}\right)\right)^{\left(\frac{1}{P_j \cdot \alpha E^{i/j}_{s/l}}\right)}\right) \tag{10}$$

$$\frac{\mathrm{C^i_r}}{\mathrm{C^i_o}} = \frac{1}{1-\mathrm{F}}\left(1 - \mathrm{P_j}\left(\frac{\mathrm{F}}{\mathrm{D^j_{s/l}}}\right)\right)^{\left(\frac{1}{\mathrm{P_j \cdot \alpha E^{i/j}_{s/l}}}\right)} \tag{11}$$

$$\frac{\mathrm{C^i_l}}{\mathrm{C^i_o}} = \frac{1}{\mathrm{D^j_{s/l}} * \alpha \mathrm{E^{i/j}_{s/l}} + \mathrm{F}(1 - \mathrm{P_j} \cdot \alpha \mathrm{E^{i/j}_{s/l}})} \tag{12}$$

$$\frac{\mathrm{C^i_r}}{\mathrm{C^i_o}} = \left(\frac{\mathrm{D^j_{s/l}} * \alpha \mathrm{E^{i/j}_{s/l}} - \mathrm{P_j} * \alpha \mathrm{E^{i/j}_{s/l}} \times \mathrm{F}}{1-\mathrm{F}}\right) \times \left(\frac{1}{\mathrm{D^j_{s/l}} * \alpha \mathrm{E^{\frac{i}{j}}_{s/l}} + \mathrm{F}(1 - \mathrm{P_j} * \alpha \mathrm{E^{i/j}_{s/l}})}\right) \tag{13}$$

$$10^3 \ln\left(\frac{\mathrm{C^i_l}}{\mathrm{C^j_l}}\right) = \delta^{\mathrm{i/j}}\mathrm{E}. \tag{14}$$

Variables used in this study are shown in Table 2. Partition coefficients of elements are from McKenzie & O'Nions (1995) and Mallmann and O'Neill (2009). The partition coefficient of Cr is sensitive to Cr^{2+}/Cr_{TOT} (Schreiber & Haskin, 1976; Roeder & Reynolds, 1991; Li et al., 1995;

Bonnand et al., 2020a,b). The partition coefficients for minerals in spinel peridotites are calculated for a mantle Cr^{2+}/Cr_{TOT} 0.15 (Table 2Berry et al., 2006; Shen et al., 2018). Melting reactions of spinel and garnet peridotites for the interval of melting from 0 to 20 % melting, are given in Table 2. The partition coefficients and melting reactions used in this study do not vary. It is assumed that this approximation holds for a compatible element like Cr over the melting range modelled (20%). The mode of spinel is more important for Cr than other elements and is calculated using the average modal abundance of fertile mantle peridotites measured in this study, (0.028, Table S5).

The bulk α-value is the weighted sum of the α-values of all minerals in the mantle (Eq. (15), where $f_{residue(x)}$ is the fraction of Cr hosted in each phase). The bulk fractionation factor will vary as the degree of melting alters the modal mineralogy of the residue and, therefore, $f_{residue(x)}$. Measurements of mineral-melt pairs provide primary $\alpha_{x\text{-melt}}$ values, however no Cr isotope measurements of primary melts in contact with their source material and residual minerals are available. Instead, the minerals-melt α-values can be modelled by comparing the $\delta^{53}Cr$ of minerals to a theoretical initial melt composition, or by comparison to theoretical equilibrium fractionation between melt and mantle minerals (Berry et al., 2021a). The fractionation factor can be used for modal and non-modal melting, depending on the melting reactions used to calculate the theoretical initial melt.

$$\alpha E_{mantle-melt} = \sum_{x} f_{residue(x)} * \alpha E_{x-melt} \quad (15)$$

Mantle mineral $\delta^{53}Cr$ compositions can, in principle, be deduced in two ways, isotopic measurements and ionic models. Fig. 3 shows the $\delta^{53}Cr$ composition of mineral separates from spinel bearing peridotites measured in this study (Table S1) and previous studies (Xia et al., 2017; Shen et al., 2018). No measurements of garnet bearing peridotites have been made. The $\Delta^{53}Cr$-values, that is the difference in $\delta^{53}Cr$ between two phases, can be used to calculate the average Cr isotopic composition of the mantle minerals. Fig. 3 shows that the range in $\Delta^{53}Cr$-values of mineral separates results in high uncertainties (2 s.d. = 0.17–0.27‰). The variations seen in the mineral pair compilation may partially be explained by different physical conditions of the peridotites; temperature and fO_2 will affect the equilibrium isotopic composition (Shen et al., 2018). However, the variations cannot entirely be explained as equilibrium features. For example, in Fig. 3b and d, both negative and positive $\Delta^{53}Cr\text{-}_{x\text{-}y}$ values are found, which cannot be produced by differences in temperature (as temperature will only affect the magnitude), or by variations in Cr oxidation state, as olivine will always have the highest Cr^{2+}/Cr_{TOT} due to the greater compatibility of Cr^{2+} in olivine (Mallmann and O'Neill, 2009). Variations could arise from non-equilibrium processes, such as diffusion or metasomatism (Shen et al., 2018; Bai et al., 2019). Whatever the mechanism, the range in $\Delta^{53}Cr$-values means that mineral measurements are unsuitable for modelling.

Ionic models can be used to calculate equilibrium isotopic fractionations under set conditions. Shen et al., (2018) calculated isotopic compositions of minerals in spinel lherzolites, using the Cr^{2+}/Cr_{TOT} and the coordination number to calculate the potential energy of the site that Cr inhabits. The relative $\delta^{53}Cr$ composition of mantle minerals from measurements is the same as the theoretical values calculated for a mantle peridotite with $Cr^{2+}/Cr_{TOT} = 0.15$ Shen et al. (2018) i.e., spinel > cpx = opx > olivine.. The composition of garnet was not calculated in Shen et al., (2018). However, the expected value can be inferred using their calculations. Garnet contains Cr^{3+} in octahedral sites (Carlson, 2012), which for the ionic model of (Shen et al., 2018) is analogous to Cr^{3+} in spinel and olivine. Therefore, the same potential energy is assumed to be applicable for Cr^{3+} in garnet.

The α-values can be converted into $\Delta^{53}Cr_{mantle\text{-}melt}$ values to clearly show difference in isotopic composition between phases. Mineral-melt $\Delta^{53}Cr_{mantle\text{-}melt}$ -values are calculated using the modelled equilibrium mineral compositions of garnet- and spinel-bearing peridotite and the melting conditions in Table 2. The modal mineral abundance of the residue is then used to calculate the $\Delta^{53}Cr_{mantle\text{-}melt}$ -value as a function of melting (Fig. 4). The initial values

Table 2
Partition coefficients taken from (McKenzie and O'Nions, 1995; Liu and O'Neill, 2004; Mallmann and O'Neill, 2009). A spinel modal abundance of 0.028 is calculated from the average value for fertile spinel lherzolites (Supplementary Information.). Melting reactions and modes are taken from Sossi & O'Neill, 2017, Gudfinnsson & Presnall, 1996 and Walter, 1998. Partition coefficients for Cr are for $Cr^{2+}/Cr_{TOT} = 0.15$, which is an estimate for the Cr^{2+}/Cr_{TOT} ratio during melting of the terrestrial mantle (Berry et al., 2006; Shen et al., 2018).

	Olivine	Orthopyroxene	Clinopyroxene	Spinel	Garnet
$D_{mineral\text{-}melt}(Cr^{2+})$	0.85	0.84	0.59	–	–
$D_{mineral\text{-}melt}(Cr^{3+})$	0.85	3.52	12.6	170	5.5
$D_{mineral\text{-}melt}$ $(Cr^{2+}/Cr_{TOT} = 0.15)$	0.85	2.98	10.20	170	5.5
Spinel peridotites					
Reaction	−0.29	0.46	0.71	0.11	–
Mode	0.589	0.235	0.147	0.028	–
ΣD = 7.4			ΣP = 28.3		
Garnet peridotites					
Reaction	0.05	−0.15	0.96	–	0.14
Mode	0.57	0.28	0.13	–	0.05
ΣD = 3.5			ΣP = 12.6		

for melt formed are lighter than the mantle by 0.09 and 0.07‰ for spinel and garnet peridotites respectively, which both become lighter with degree of melting. This agrees with measurements of partial melts - the composition of (high degree) komatiitic melts (Sossi et al., 2018; Jerram et al., 2020) is closer to the mantle value than lower degree basaltic melts (Bonnand et al., 2020a,b; Shen et al., 2020). The initial $\Delta^{53}Cr_{mantle\text{-}melt}$-value of spinel bearing peridotites is higher than garnet bearing peridotites, as residues with spinel initially contain a greater amount of isotopically heavy Cr. However, the spinel peridotite $\Delta^{53}Cr_{mantle\text{-}melt}$-value decreases, as spinel is consumed at a greater rate than garnet during non-modal melting.

The modelled $\Delta^{53}Cr_{mantle\text{-}melt}$-values agree with the average composition of basaltic suites, which are up to 0.07‰ lighter than the mantle (Bonnand et al., 2020a,b; Shen et al., 2020). The composition of basaltic melts can only provide an approximation of the $\Delta^{53}Cr_{mantle\text{-}melt}$ -value as they may not represent the first increment of melt. However, the fact that the calculated $\Delta^{53}Cr_{mantle\text{-}melt}$-values have similar composition and behaviour to partial melts, provides confidence in the calculated $\Delta^{53}Cr_{mantle\text{-}melt}$ -values. The Δ-values from theoretical equilibrium fractionations between the melt and a mantle residue, are even smaller $\Delta^{53}Cr_{mantle\text{-}melt}$ -values, < 0.01‰ (Berry et al., 2021a,b) Therefore, the composition of melts produced in the mineral melting model presents an upper limit, which would be reduced through isotopic equilibrium with the residue.

Fig. 5 compares non-modal melting models to the data for ultramafic samples. Peridotites in Fig. 5a are those that do not show clear evidence of metasomatism (see Supplementary Information). The models have a starting composition of the BSE of $\delta^{53}Cr = -0.12$‰ and use variable $\Delta^{53}Cr_{mantle\text{-}melt}$-values and D and P values given in Table 2. The $\delta^{53}Cr$ in the residual mantle in the models varies by < 0.01‰, far less than the ~ 0.3‰ variation seen in the selected peridotites. The non-modal models for spinel peridotites and garnet lherzolites both produce smaller variations than are seen in the measurements of their respective rock types. The models are totally encompassed by the range of mantle peridotite $\delta^{53}Cr$, which greatly exceeds the variability generated in the melting models. There is a slight divergence between the modelled $\delta^{53}Cr$ variations for garnet and spinel. Garnet has a lower Cr partition coefficient than spinel (McKenzie & O'Nions, 1995; Mallmann and O'Neill, 2009), however spinel is removed at a greater rate from the mantle during non-modal melting. This results in the $\delta^{53}Cr$ of residual spinel facies mantle being slightly more susceptible to partial melting.

The modelled composition of melts is presented in Fig. 5b, alongside the average or initial composition of basaltic suites (Bonnand et al., 2020a,b; Shen et al., 2020). The modelled variability lies within the range of basalts ($\delta^{53}Cr = -0.19$ to -0.12‰), demonstrating that the behaviour of Cr is well approximated using this model. The small variable α-values calculated in this study, are able to recreate the composition of natural melts, even though they only produce small $\delta^{53}Cr$ variations in the residue of < 0.01‰. The composition of melts formed from garnet and spinel peridotites show little variation with degree of melting (~0.03‰) and the melts formed are within < 0.02 ‰ for all increments of melting. The composition of initial basaltic melts show a greater variation than the models (Fig. 5), which cannot be explained by degree of melting alone. Melting in the mantle occurs at different temperatures and oxidation states, which affects the magnitude of equilibrium fractionation. The model presented in Fig. 5 uses values that provide the best overall representation of the mantle. However, variations in natural conditions are expected, which could produce the range in the composition of initial melts. Fig. 3 shows that there is heterogeneity in the $\delta^{53}Cr$ composition of minerals in the mantle, which could also produce different $\Delta^{53}Cr_{mantle\text{-}melt}$-values. However, the sensitivity tests (Supplementary Information) show that even if the $\Delta^{53}Cr_{mantle\text{-}melt}$-value is slightly higher, the composition of the residue will still not be significantly affected.

The models presented here show that the variation of $\delta^{53}Cr$ in the mantle cannot be explained by non-modal partial melting over the degrees considered. The small $\Delta^{53}Cr_{mantle\text{-}melt}$-values close to zero, together with the compatible nature of Cr in the mantle, means that the $\delta^{53}Cr$ variation in the mantle resulting from partial melting is small. This agrees with models and data for other compatible elements, such as Ni (Klaver et al., 2020; Saunders et al., 2020), and is in contrast to the behaviour of V and Fe which show variations (Williams et al., 2005; Weyer and Ionov, 2007; Prytulak et al., 2013). Previous models of $\delta^{53}Cr$ evolution in the mantle (Xia et al., 2017; Shen et al., 2018) produce larger estimates of melting-induced variation likely due to the choice of smaller partition coefficients, resulting in more Cr removed from the mantle, and higher $\Delta^{53}Cr_{mantle\text{-}melt}$ -values. These parameters result in more Cr removed from the mantle through melting, which, combined with the larger isotopic fractionation, makes the mantle more susceptible to melting. The differences between the non-modal melting models produced here and those of other studies are discussed further in the Supplementary Information. The modelling carried out in this section is applicable to low to medium degree melts only, as the behaviour of Cr (melting reactions and partition coefficients) at higher degrees of melting is less well constrained. However, high degree partial melts (komatiites) have $\delta^{53}Cr$ compositions similar to the BSE (Jerram et al., 2020), therefore, only small changes in the mantle may be anticipated at high degrees of melting as well.

5.2. Statistical tests on the $\delta^{53}Cr$ of mantle peridotites

To understand further the effect of partial melting, the model results are compared with statistical analyses of the variations in $\delta^{53}Cr$ associated with a population of samples exhibiting chemical characteristics consistent with different degrees of melt depletion. Samples selected for the statistical tests should not display petrographic or trace element effects of processes other than partial melting. Thirty-eight of the samples measured in this study are sufficiently well-characterised in terms of their petrology and geochemistry to be considered for inclusion in linear regression and two tailed Student's *t* statistical tests (see Supplementary

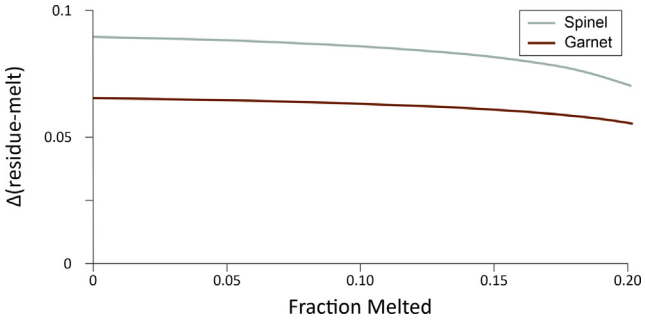


Fig. 4. Variable Δ-values for spinel and garnet bearing peridotites as a function of melt fraction. Values are calculated using model equilibrium mineral compositions and melting reactions (Gudfinnsson & Presnall, 1996; Walter, 1998; Sossi & O'Neill, 2017; Shen et al., 2018). Greater variation is seen for spinel bearing peridotites, however the values are similar for both spinel and garnet bearing peridotites.

Information). Of these, 8 samples exhibited textures created by metasomatic and contamination processes. A further 7 samples were excluded on the basis of their chemical composition, either due to high $(La/Yb)_N$ ratios or Ca/Al ratios that deviated from a simple melting trend (Fig. S4). The remaining 23 mantle peridotites have strongly correlated indicators of melting (Fig. S5). These samples along with 12 mantle peridotites identified as unmetasomatised in Xia et al. (2017) were included in the dataset of selected peridotites.

Aluminium can be used as a proxy for partial melting, as the bulk distribution coefficient is robust to changes in temperature and pressure (Herzberg, 2004; Ionov & Hofmann, 2007). Aluminium is also immobile during weathering, serpentinization and metamorphism (Coleman and Keith, 1971; Snow and Dick, 1995). Variations of Al_2O_3 (wt.%) can occur through interactions with silicate melts (Le Roux et al., 2007), however, the strong correlation between Al_2O_3 (wt.%) and other indicators of partial melting (CaO wt.%, cpx % and Mg#), and suggest that the composition of our selected samples reflects partial melting (Fig. S5).

Variations in $\delta^{53}Cr$ as a function of Al_2O_3 (wt.%) for the 35 selected mantle peridotites are shown in Fig. S6a. There is no correlation between $\delta^{53}Cr$ and degree of partial melting. Similarly, low R^2 values are calculated for $\delta^{53}Cr$ and other indicators of melting (CaO wt.%, cpx % and Mg#; Fig. S6). It should be noted however, that a previous study found a stronger correlation between Al_2O_3 and $\delta^{53}Cr$ in peridotites with an R^2 of 0.35 given by Xia et al. (2017). Therefore, further work is needed to understand why there is this apparent difference.

The selected set of mantle peridotites can also be used to carry out Student's T tests, which can reveal melting induced $\delta^{53}Cr$ variations that do not produce a linear correlation. For example, if significant variations in $\delta^{53}Cr$ only occur at < 2 % Al_2O_3 wt.% this may not produce a linear correlation but will produce a statistically significant difference in composition between refractory and fertile mantle peridotites. The statistical test was carried out by splitting the selected peridotites into 4 groups with an equal number of samples, using an indicator of partial melting (Al_2O_3 wt. %, Mg# and CaO wt.%). The Student's double tailed t-test was then carried out between the most fertile and most depleted of these groups. At the 95 % confidence level there is no evidence to suggest that there is a difference in $\delta^{53}Cr$ between the most fertile and most depleted mantle peridotites (see Supplementary Material for detailed discussion). Again, this contrasts with the results of Xia et al. (2017) who found $\sim 0.1‰$ differences between peridotites with $Al_2O_3 > 3$ % and < 3 %.

The statistical tests find no evidence that the Cr isotopic composition of the upper mantle is affected by any degree of partial melting. This is consistent with the measured compositions of melt extracted at higher degrees of melting. Komatiites have indistinguishable $\delta^{53}Cr$ from the composition of the BSE (Sossi et al., 2018; Jerram et al., 2020). Small differences in the compositions of melts are expected, and time series experiments have also shown that disequilibrium melting can fractionate Cr isotopes (Bonnand et al., 2020a,b). However, as there is no relation between $\delta^{53}Cr$ and degree of partial melting, this process cannot cause resolvable variations in the $\delta^{53}Cr$ of the residue. Other disequilibrium mantle processes, are addressed in the following section.

5.3. Explanations for $\delta^{53}Cr$ heterogeneity in mantle peridotites

Ten mantle peridotites measured in this study are isotopically lighter and 11 heavier than the BSE ($\delta^{53}Cr = -0.12 \pm 0.04‰$, Jerram et al. 2020). There also are resolvable differences between mantle peridotites that fall within the range of the BSE. If partial melting does not create resolvable changes to the $\delta^{53}Cr$ of mantle peridotites, other explanations must be found for the significant variations (Fig. 2). Broadly speaking there are two kinds of processes, other than melting, that might impact transition element isotopic composition in the mantle – recycling of subducted sediment or crust and disequilibrium kinetic fractionation.

Recycling of subducted sediments and crust, which can be isotopically fractionated at low temperatures, may dominate some isotope systems, such as K (Tuller-Ross et al., 2019). Low temperature processes can fractionate $\delta^{53}Cr$, with some sediments recording compositions of $> 0.4‰$ (Frei et al., 2009; Bonnand et al., 2013; Gueguen et al., 2016; Holmden et al., 2016; Frank et al., 2020). Igneous silicate rocks have a smaller range in $\delta^{53}Cr$ values of -0.22 to

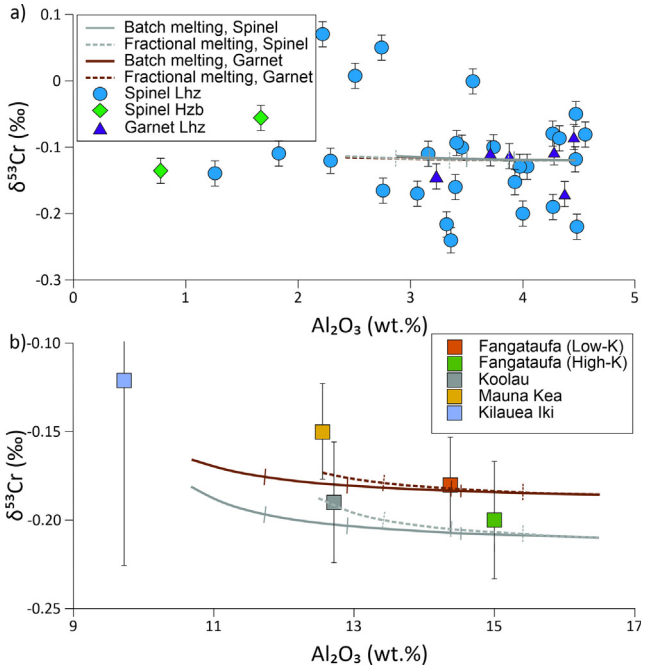


Fig. 5. The $\delta^{53}Cr$ versus Al_2O_3 (wt.%) for selected mantle peridotites (this study and Xia et al. 2017) compared to modelled mantle evolution lines for partial melts are shown in 5a. Fig. 5b shows the average composition of basaltic suites (Shen et al., 2020), or in the case of Fangataufa (Low-K) basalts the calculated initial composition (Bonnand et al., 2020a,b). The models use the starting given in Table 2.

0.00‰, resulting from partial melting and crystallisation (Schoenberg et al., 2008; Bonnand et al., 2020a,b; Shen et al., 2020). Therefore, in principle, incorporation of recycled material into the mantle can impose localised variations in $\delta^{53}Cr$. However, the low Cr concentrations in sediment and crust compared with those in the mantle will prevent large changes in $\delta^{53}Cr$, simply from a mass balance consideration. To affect the Cr isotopic compositions significantly would require a mass of recycled material that would drastically alter the composition of mantle peridotites by increasing the concentration of incompatible elements, (e.g., K, Ba, U etc.). However, there is no correlation between $\delta^{53}Cr$ and the concentrations of these elements.

Kinetic isotope fractionation, disequilibrium effects and metasomatic interactions have been implicated in causing large isotopic variations in mantle peridotite for many transition elements, (e.g. Fe, Ni and Zn; Weyer & Ionov, 2007; Wang et al., 2017; Klaver et al., 2020), as well as Cr (Xia et al., 2017; Shen et al., 2018). Differences of $\delta^{53}Cr = 0.8‰$ have been explained in these ways, leading to both isotopically light and heavy peridotites. Xia et al. (2017) explained isotope heterogeneities in peridotites through isotopically light Cr diffusing from Cr-rich peridotites into silicate melts, which in turn crystallised isotopically light pyroxenite cumulates in melt channels. This created a $\delta^{53}Cr$ gradient with lightest values in the melt-filled vein and surrounding mantle, and isotopically heavier values reaching a maximum at some distance away from the vein. Apart from isotopically heavy Cr, peridotites modified in this fashion did not show anomalous chemical compositions. The pyroxenite (P6) measured in this study, has a $\delta^{53}Cr$ lighter than the BSE ($\delta^{53}Cr = -0.35‰$) which may result from similar interactions. No other mantle samples in this study relate to P6. However, it is possible that interactions with similar silicate melts contributed to the $\delta^{53}Cr$ of some mantle peridotites in this study.

Variations in the $\delta^{53}Cr$ of mantle peridotites have also been attributed to the introduction of low degree partial melts (Shen et al., 2018). Metasomatism by low degree partial melts in the mantle is widespread, including by kimberlitic (e.g. Menzies & Wass, 1983) and carbonatitic (Yaxley et al., 1991; Ionov et al., 1993a,b; Griffin et al., 1996) melts. These interactions are recorded by elevated light REE to heavy REE ratios such as $(La/Yb)_N$ (Green and Wallace, 1988; Rudnick et al., 1993), due to the incompatible element enriched composition of low degree partial melts (Baker et al., 1995). Thirteen of the fourteen LREE-enriched ($(La/Yb)_N > 1$) peridotites in this study display a similar range of $(La/Yb)_N$ as other peridotites affected by low degree partial melts (Rudnick et al., 1993). One peridotite sample (4500-18) has an extremely elevated $(La/Yb)_N$ of 61.7. The remainder display a clear positive linear co-variation between $(La/Yb)_N$ and $\delta^{53}Cr$ (Fig. 6).

There are no published $\delta^{53}Cr$ compositions of low degree partial melts but they are likely to be slightly lighter than the mantle, as are basalts (Bonnand et al., 2020a,b; Shen et al., 2020). However, equilibrium peridotite-melt $\delta^{53}Cr$ fractionations are small and, as discussed above, low degree partial melts form with composition $\leq 0.07‰$ lighter than the composition of the BSE. Therefore, non-equilibrium fractionation is a more plausible mechanism for low degree partial melts to alter the $\delta^{53}Cr$ of mantle peridotites. Due to the relatively low Cr contents of low degree partial melts such a hypothetical process would require a large volume of melt, or a large fractionation. A

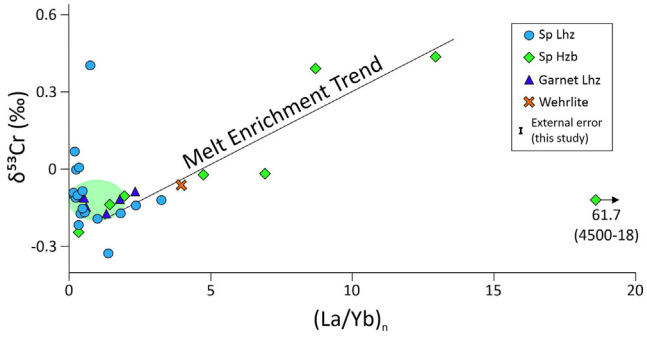


Fig. 6. $(La/Yb)_N$ versus $\delta^{53}Cr$ of mantle peridotites measured in this study. A $(La/Yb)_N$ /$\delta^{53}Cr$ trend is identified, which contains 13 samples with $(La/Yb)_N > 1$ that have a strong correlation with $\delta^{53}Cr$, as highlighted by the melt enrichment trend ($R^2 = 0.86$). The light blue circle represents the composition of the BSE. (For interpretation of the references to colour in this figure legend, the reader is referred to the web version of this article.)

process that could create large fractionations in the mantle would be disequilibrium Cr exchange during chromatographic migration of liquids through the mantle. Mantle chromatography has previously been used to explain decoupling between elements (Ionov & Hofmann, 1995; Ionov et al., 2002) and is thought to occur during interactions between a column of melt and the mantle. If an element in the melt is over- or under-saturated with respect to the mantle, a chemical potential gradient can be created, that will result in an exchange of that element until equilibrium is reached or the melt is removed (Navon and Stolper, 1987).

Mantle chromatography is particularly relevant to low degree partial melts such as carbonatites. Some of the samples with $(La/Yb)_N > 1$ also show fractionated Ti/Eu (Fig. 7), which is considered diagnostic of carbonatite metasomatism (Nelson et al., 1988; Rudnick et al., 1993; Sweeney, 1994; Yaxley et al., 1998). Experimental data show that $D_{Cr\ Mantle\text{-}Carbonatite}$ greatly increases from 0.5 to 9 GPa as shown in Fig. S7. Transient carbonatite melts decompressing while rising through the mantle, may not reach equilibrium with the surrounding peridotite, but will become undersaturated in Cr with respect to the mantle, therefore fulfilling the prerequisites of mantle chromatography (Navon and Stolper, 1987). As the melts rise and interact with the mantle, there will be a transfer of Cr into the undersaturated component, the carbonatite liquid. Large changes in the $\delta^{53}Cr$ may occur, due to kinetic fractionation, as isotopically light isotopes diffuse faster into melt (Richter et al., 2009), if this process does not reach equilibrium (i.e. the interaction is transient). High Cr diffusion rates are required for this method. The thermal diffusion of Cr in mantle minerals occurs over billion year timescales (e.g. Ganguly et al., 2007). However, diffusion due to chemical gradients on relevant timescales has been observed; fluid/melt metasomatism has been implicated in causing diffusion of Cr in spinel cores (El Dien et al., 2019).

This process can be illustrated through mass balance calculations. The calculations used are described in greater detail in the Supplementary Information. Fig. S8 shows the results of 3 scenarios that can produce a mantle peridotite with $\delta^{53}Cr = 0.43‰$ through disequilibrium Cr exchange. Briefly, higher $\delta^{53}Cr$ of the altered mantle is favoured by: 1) an isotopically light carbonatite product (the final composition of the carbonatite liquid after the disequilibrium exchange), 2) the removal of larger amounts (up to 500 $\mu g.g^{-1}$) of Cr from the mantle peridotite, 3) increasing the carbonatite/peridotite ratio (up to 5 is modelled). The isotopically heaviest $\delta^{53}Cr$ mantle peridotites were likely created by an interaction that takes a midpoint between these scenarios. Most samples with $(La/Yb)_N > 1$ could be produced by a smaller extent of interaction. Therefore, a pervasive flux of carbonatite melt transfer perhaps over many millions of years could progressively change the isotopic composition of localised mantle peridotites with only a modest increase of 20 $\mu g.g^{-1}$in Cr concentration in the carbonatite, and a $\delta^{53}Cr$ similar to the pyroxenite veins in Xia et al., (2017). Such low Cr, low degree partial melts, do not introduce Cr into the residual mantle but do provide a repository for isotopically light Cr, which will change the mantle $\delta^{53}Cr$.

Although this process may explain the relationship between $(La/Yb)_N$ and $\delta^{53}Cr$, only the LREE enriched samples lie on this trend (Fig. 6), while samples that show no LREE enrichments may have $\delta^{53}Cr$ values beyond the BSE range. Therefore, other processes must also be involved. The metasomatic change of $\delta^{53}Cr$ will be accompanied by only limited changes to the bulk major element composition (see also Xia et al. 2017). If, subsequently, the melt-affected peridotites are disturbed by repeated small degrees of fractional partial melting, then, in principle, it seems plausible that the La will be preferentially lost. The only noticeable effect surviving from earlier melt-rock interactions would be the $\delta^{53}Cr$ composition. This might explain the variation in mantle peridotites that have $(La/Yb)_N < 1$. This subset has a strikingly similar range in $\delta^{53}Cr$ to mantle peridotites with $(La/Yb)_N > 1$ (−0.24 to 0.40‰ and −0.33 to 0.43‰ respectively). Yet for these samples, no correlation with $(La/Yb)_N$ or other geochemical parameters, including indicators of partial melting, are apparent.

It should also be noted that some of the most isotopically heavy $\delta^{53}Cr$ samples are melt depleted harzburgites or low-Al_2O_3 lherzolites. As discussed above, melt depleted samples do not form part of a melting trend with $\delta^{53}Cr$. It has previously been suggested that harzburgites and other melt depleted samples are more susceptible to metasomatism (Bodinier et al., 1990). If these effects extend to the loss of light Cr, then this may explain why harzburgites appear

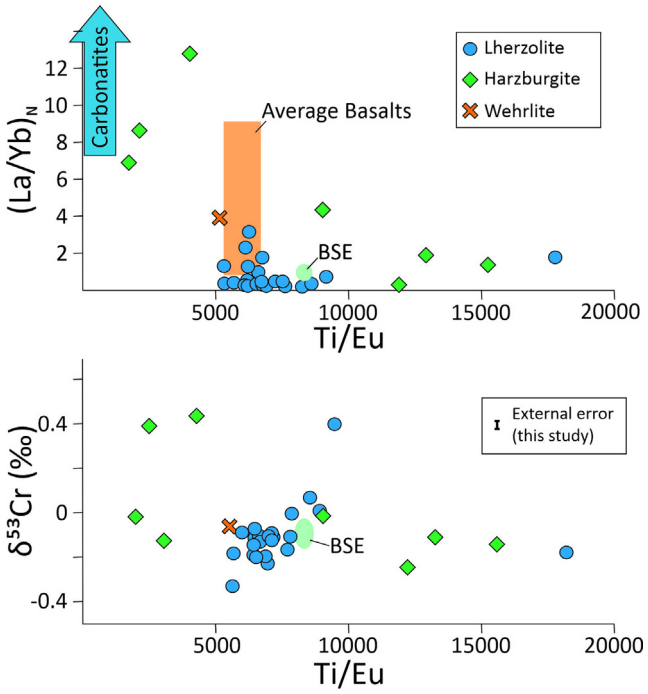


Fig. 7. Showing Ti/Eu against a) $(La/Yb)_N$ and b) $\delta^{53}Cr$. The composition of the BSE is given by the green oval and the range in the average compositions N-MORB, E-MORB and IAB basalts is provided by the orange rectangle using values from (Sun and McDonough, 1989);$(La/Yb)_N = 0.45–9$ and Ti/Eu = 5300–6700). Many of the samples lie out of this range.

to be more susceptible to enrichment of heavy Cr isotopes. Alternatively, it may be that there are other explanations related to aspects of Cr behaviour that are not yet well enough understood.

The discussion on $\delta^{53}Cr$ behaviour in mantle processes has thus far focussed on the production of the heavier $\delta^{53}Cr$ of mantle peridotites. Light $\delta^{53}Cr$ compositions have been measured in pyroxenites with 1000–4000 $\mu g.g^{-1}$ Cr (Xia et al., 2017). The high Cr content of pyroxenites and their isotopically light compositions, means that this lithology may have further implications for the $\delta^{53}Cr$ of the mantle. These isotopically light magmas would themselves produce lighter mantle compositions if they were to interact with peridotites. There are few isotopically light peridotites in the dataset, which implies that this process would not be as widespread.

Finally, although metasomatism normally is not considered to greatly impact compatible elements concentrations, metasomatised peridotites also record isotopically heavy and light Ni compositions (Klaver et al., 2020; Saunders et al., 2020). There is therefore increasing evidence that the isotope composition and bulk concentration of compatible elements become decoupled because of metasomatic effects.

6. CONCLUSIONS

(1) The $\delta^{53}Cr$ of diverse mantle peridotites studied here define a range from −0.33 to 0.44‰.

(2) Modelling shows that the Cr isotope composition of the upper mantle will not significantly change by melting over a range of realistic partition coefficients and $\Delta^{53}Cr_{mantle\text{-}melt}$-values. A change in $\delta^{53}Cr$ of the mantle residue of < 0.01‰ is expected at ≤ 20 % melting, far less than the variations observed in peridotite xenoliths.

(3) Consistent with this, the $\delta^{53}Cr$ compositions of the peridotites display no robust correlation with indicators of partial melting such as Al_2O_3, CaO, Mg# and clinopyroxene abundance, and no statistically significant difference is observed between fertile and melt depleted peridotites.

(4) Nearly all of the LREE-enriched samples in this study display a co-variation between $(La/Yb)_N$ and $\delta^{53}Cr$. This provides evidence that some form of interaction with low degree partial melts may have led to disequilibrium loss of light Cr from the mantle peridotites into a transient melt phase, through mantle chromatography.

(5) Perturbations in $\delta^{53}Cr$ may be preserved in the mantle over long periods of Earth history, because other processes such as melting are unable to change the isotopic compositions further. However, subsequent melting would affect LREEs, which may partially explain the similar range of Cr isotope variability found in LREE depleted samples.

(6) In principle, metasomatic interactions can generate isotopically heavy and light $\delta^{53}Cr$ as found in mantle peridotites. This is consistent with evidence from Ni

isotopes and provides evidence that compatible element isotope variations in the mantle due to non-equilibrium melt-rock reactions may be pervasive.

Declaration of Competing Interest

The authors declare that they have no known competing financial interests or personal relationships that could have appeared to influence the work reported in this paper.

ACKNOWLEDGMENTS

Research funding for this work was provided by the Science and Technology Facilities Council (STFC) to A. N.H. (STFC Planetary Origins and Developments: ST/M001318/1). We thank Phil Holdship and Alan Hsieh for providing instrumental support, and to Jane Barling and Steve Wyatt for laboratory support. We would also like to thank Paolo Sossi and two anonymous reviewers for their help with the manuscript.

Data supporting the publication can be accessed by contacting MJ.

APPENDIX A. SUPPLEMENTARY MATERIAL

Supplementary data to this article can be found online at https://doi.org/10.1016/j.gca.2021.10.022.

REFERENCES

Albaréde F. and Beard B. (2004) Analytical methods for non-traditional isotopes. *Rev. Mineral.* **55**, 74.

Bai Y., Su B., Xiao Y., Chen C., Cui M., He X.-Q., Qin L. and Charlier B. (2019) Diffusion-driven chromium isotope fractionation in ultramafic cumulate minerals: Elemental and isotopic evidence from the Stillwater Complex. *Geochim. Cosmochim. Acta* **263**, 167–181.

Baker M. B., Hirschmann M. M., Ghiorso M. S. and Stolper E. M. (1995) Compositions of near-solidus peridotite melts from experiments and thermodynamic calculations. *Nature* **375**, 308–311.

Baker M. B. and Stolper E. M. (1994) Determining the composition of high-pressure mantle melts using diamond aggregates. *Geochim. Cosmochim. Acta* **58**, 2811–2827.

Berry A. J., Miller L. A., O'Neill H. St. C. and Foran G. J. (2021a) The coordination of Cr^{2+} in silicate glasses and implications for mineral-melt fractionation of Cr isotopes. *Chem. Geol.*, 120483.

Berry A. J., O'Neill H., St C. and Foran G. J. (2021b) The effects of temperature and pressure on the oxidation state of chromium in silicate melts. *Contrib. Mineral. Petrol.* **176**, 1–14.

Berry A. J., O'Neill H., St C., Scott D. R., Foran G. J. and Shelley J. M. G. (2006) The effect of composition on Cr^{2+}/Cr^{3+} in silicate melts. *Am. Mineral.* **91**, 1901–1908.

Bodinier J. L., Vasseur G., Vernieres J., Dupuy C. and Fabries J. (1990) Mechanisms of mantle metasomatism: Geochemical evidence from the lherz orogenic peridotite. *J. Petrol.* **31**, 597–628.

Bonnand P., Bruand E., Matzen A. K., Jerram M. and Schiavi F. (2020a) Redox control on chromium isotope behaviour in silicate melts in contact with magnesiochromite. *Geochim. Cosmochim. Acta* **288**, 282–300.

Bonnand P., Doucelance R., Boyet M., Bachèlery P., Bosq C., Auclair D. and Schiano P. (2020b) The influence of igneous processes on the chromium isotopic compositions of terrestrial basalts. *Earth Planet. Sci. Lett.* **532** 116028.

Bonnand P. and Halliday A. N. (2018) Oxidized conditions in iron meteorite parent bodies. *Nat. Geosci.* **11**, 2–6.

Bonnand P., James R. H., Parkinson I. J., Connelly D. P. and Fairchild I. J. (2013) The chromium isotopic composition of seawater and marine carbonates. *Earth Planet. Sci. Lett.* **382**, 10–20.

Bonnand P., Parkinson I. J. and Anand M. (2016) Mass dependent fractionation of stable chromium isotopes in mare basalts: Implications for the formation and the differentiation of the Moon. *Geochim. Cosmochim. Acta* **175**, 208–221.

Bonnand P., Parkinson I. J., James R. H., Karjalainen A.-M. and Fehr M. A. (2011) Accurate and precise determination of stable Cr isotope compositions in carbonates by double spike MC-ICP-MS. *J. Anal. At. Spectrom.* **26**, 528–535.

Carlson W. D. (2012) Rates and mechanism of Y, REE, and Cr diffusion in garnet. *Am. Mineral.* **97**, 1598–1618.

Coleman R. G. and Keith T. E. (1971) A chemical study of serpentinization — Burro Mountain, California. *J. Petrol.* **12**, 311–328.

Dauphas N., Craddock P. R., Asimow P. D., Bennett V. C., Nutman A. P. and Ohnenstetter D. (2009) Iron isotopes may reveal the redox conditions of mantle melting from Archean to Present. *Earth Planet. Sci. Lett.* **288**, 255–267.

Davies R., Nixon P. H., Pearson G. and Obata M. (1993) Tectonic implications of graphitized diamonds from the Ronda peridotite massif, southern Spain. *Geology* **21**, 2–5.

El Dien H. G., Arai S., Doucet L., Li Z., Kil Y., Fougerouse D., Reddy S. M., Saxey D. W. and Hamdy M. (2019) Cr-spinel records metasomatism not petrogenesis of mantle rocks. *Nat. Commun.* **10**, 1–12.

Downes H. (2007) Origin and significance of spinel and garnet pyroxenites in the shallow lithospheric mantle: Ultramafic massifs in orogenic belts in Western Europe and NW Africa. *Lithos* **99**, 1–24.

Drake M. J., Newsom H. E. and Capobianco C. J. (1989) V, Cr, and Mn in the Earth, Moon, EPB, and SPB and the origin of the Moon: Experimental studies. *Geochim. Cosmochim. Acta* **53**, 2101–2111.

Ellis A. S., Johnson T. M. and Bullen T. D. (2002) Chromium Isotopes and the Fate of Hexavalent Chromium in the Environment. *Science (80-.)* **295**, 2060–2062.

Farkaš J., Chrastný V., Novák M., Čadkova E., Pasava J., Chakrabarti R., Jacobsen S. B., Ackerman L. and Bullen T. D. (2013) Chromium isotope variations ($\delta^{53}/^{52}Cr$) in mantle-derived sources and their weathering products: Implications for environmental studies and the evolution of $\delta^{53}Cr/^{52}Cr$ in the Earth's mantle over geologic time. *Geochim. Cosmochim. Acta* **123**, 74–92.

Frank A. B., Klaebe R. M., Löhr S., Xu L. and Frei R. (2020) Chromium isotope composition of organic-rich marine sediments and their mineral phases and implications for using black shales as a paleoredox archive. *Geochim. Cosmochim. Acta* **270**, 338–359.

Frei R., Gaucher C., Poulton S. W. and Canfield D. E. (2009) Fluctuations in Precambrian atmospheric oxygenation recorded by chromium isotopes. *Nature* **461**, 250–253.

Ganguly J., Ito M. and Zhang X. (2007) Cr diffusion in orthopyroxene: Experimental determination, ^{53}Mn–^{53}Cr thermochronology, and planetary applications. *Geochim. Cosmochim. Acta* **71**, 3915–3925.

Gibson S. A., Mcmahon S. C., Day J. A. and Dawson J. B. (2013) Highly refractory lithospheric Mantle beneath the T anzanian

Craton: Evidence from Lashaine Pre-metasomatic Garnet-bearing Peridotites. *J. Petrol.* **54**, 1503–1546.
Green D. H. and Wallace M. E. (1988) Mantle metasomatism by ephemeral carbonatite melts. *Nature* **336**, 459–462.
Griffin W. L., Smith D., Ryan C. G., O'Reilly S. Y. and Win T. T. (1996) Zoning in Mantle Minerals: and thermal events in the upper. *Can. Mineral.* **34**, 1179–1193.
Gudfinnsson H. and Presnall C. (1996) Melting relations of model lherzolite in the system CaO-MgO-Al_2O_3-SiO_2 at 2.4-3.4 GPa and the genreation of komatiites. *J. Geophyiscal Res.* **101**, 701–709.
Gueguen B., Reinhard C. T., Algeo T. J., Peterson L. C., Nielsen S. G., Wang X., Rowe H. and Planavsky N. J. (2016) The chromium isotope composition of reducing and oxic marine sediments. *Geochim. Cosmochim. Acta* **184**, 1–19.
Harvey J., Dale C. W., Gannoun A. and Burton K. W. (2011) Osmium mass balance in peridotite and the effects of mantle derived sulfides on basalt petrogenesis. *Geochim. Cosmochim. Acta* **75**, 5574–5596.
Harvey J., König S. and Luguet A. (2015) The effects of melt depletion and metasomatism on highly siderophile and strongly chalcophile elements: S-Se-Te-Re-PGE systematics of peridotite xenoliths from Kilbourne Hole, New Mexico. *Geochim. Cosmochim. Acta* **166**, 210–233.
Harvey J., Yoshikawa M., Hammond S. J. and Burton K. W. (2012) Deciphering the trace element characteristics in Kilbourne hole peridotite xenoliths: Melt-rock interaction and metasomatism beneath the Rio Grande Rift, SW USA. *J. Petrol.* **53**, 1709–1742.
Herzberg C. (2004) Geodynamic information in peridotite petrology. *J. Petrol.* **45**, 2507–2530.
Holmden C., Jacobson A. D., Sageman B. B. and Hurtgen M. T. (2016) Response of the Cr isotope proxy to Cretaceous Ocean Anoxic Event 2 in a pelagic carbonate succession from the Western Interior Seaway. *Geochim. Cosmochim. Acta* **186**, 277–295.
Ionov D. A. (2004) Chemical variations in peridotite xenoliths from Vitim, Siberia : Inferences for REE and Hf behaviour in the garnet-facies upper mantle. *J. Petrol.* **45**, 343–367.
Ionov D. A., Ashchepkov I. V., Stosch H. G., Witt-Eickschen G. and Seck H. (1993a) Garnet peridotite xenoliths from the Vitim volcanic field, Baikal Region: the nature of the garnet-spinel peridotite transition zone in the Continental Mantle. *J. Petrol.* **34**, 1141–1175.
Ionov D. A. (2007) Compositional variations and heterogeneity in fertile lithospheric mantle: peridotite xenoliths in basalts from Tariat, Mongolia. *Contrib. Mineral. Petrol.* **154**, 455–477.
Ionov D. A., Ashchepkov I. and Jagoutz E. (2005a) The provenance of fertile off-craton lithospheric mantle: Sr-Nd isotope and chemical composition of garnet and spinel peridotite xenoliths from Vitim, Siberia. *Chem. Geol.* **217**, 41–75.
Ionov D. A., Chanefo Æ. I. and Bodinier J. (2005b) Origin of Fe-rich lherzolites and wehrlites from Tok, SE Siberia by reactive melt percolation in refractory mantle peridotites. *Contrib. Mineral. Petrol.* **150**, 335–353.
Ionov D. A., Chazot G., Chauvel C., Merlet C. and Bodinier J. (2006) Trace element distribution in peridotite xenoliths from Tok, SE Siberian craton: A record of pervasive, multi-stage metasomatism in shallow refractory mantle. *Geochim. Cosmochim. Acta* **70**, 1231–1260.
Ionov D. A., Dupuy C., O'Reilly S. Y., Kopylova M. G. and Genshaft Y. S. (1993b) Carbonated peridotite xenoliths from Spitsbergen: implications for trace element signature of mantle carbonate metasomatism. *Earth Planet. Sci. Lett.* **119**, 283–297.
Ionov D. A. and Hofmann A. W. (2007) Depth of formation of subcontinental off-craton peridotites. *Earth Planet. Sci. Lett.* **261**, 620–634.
Ionov D. A. and Hofmann A. W. (1995) Nb-Ta-rich mantle amphiboles and micas: Implications for subduction-related metasomatic trace element fractionations. *Earth Planet. Sci. Lett.* **131**, 341–356.
Ionov D. A., Mukasa S. B. and Bodinier J. (2002) Sr-Nd-Pb isotopic compositions of peridotite xenoliths from Spitsbergen: numerical modelling indicates Sr-Nd decoupling in the mantle by melt percolation metasomatism. *J. Petrol.* **43**, 2261–2278.
Jerram M., Bonnand P., Kerr A. C., Nisbet E. G., Puchtel I. S. and Halliday A. N. (2020) The δ^{53}Cr isotope composition of komatiite flows and implications for the composition of the bulk silicate Earth. *Chem. Geol.* **551**, 1–13.
Kelemen P. B., Hirth G., Shimizu N., Spiegelman M. and Dick H. J. B. (1997) A review of melt migration processes in the adiabatically upwelling mantle. *Phil. Trans. A R. Soc.* **355**, 283–318.
Kelemen P. B., Shimizu N. and Salters V. J. M. (1995) Extraction of mid-ocean-rdige basalt from the upwelling mantle by focused flow of melt in dunite channels. *Nature* **375**, 747–753.
Klaver M., Ionov D. A., Takazawa E. and Elliott T. (2020) The non-chondritic Ni isotope composition of Earth's mantle. *Geochim. Cosmochim. Acta* **268**, 405–421.
Le Roux V., Bodinier J.-L., Tommasi A., Alard O., Dautria J.-M., Vauchez A. and Riches A. J. V. (2007) The Lherz spinel lherzolite: Refertilized rather than pristine mantle. *Earth Planet. Sci. Lett.* **259**, 599–612.
Lee D., Halliday A. N., Davies G. R., Essene E. J., Fitton J. G. and Temdjim R. (1996) Melt enrichment of shallow depleted mantle: a detailed petrological, trace element and isotopic study of mantle-derived xenoliths and megacrysts from the Cameroon line. *J. Petrol.* **37**, 415–441.
Li J.-P., O'Neill H., St C. and Seifert F. (1995) Subsolidus phase relations in the system MgO-SiO_2-Cr-O in equilibrium with metallic Cr, and their significance for the petrochemistry of chromium. *J. Petrol.* **36**, 107–132.
Liang Y. and Elthon D. (1990) Evidence from chromium abundances in mantle rocks for extraction of picrite and komatiite melts. *Lett. Nat.* **348**, 551–553.
Liu X. I., O'Neill H. S. and C (2004) The effect of Cr_2O_3 on the partial melting of spinel lherzolite in the system CaO–MgO–l_2O_3–SiO_2–Cr_2O_3 at 1.1 GPa. *J. Petrol.* **45**, 2261–2286.
Mallmann G., O'Neill H. St. and C (2009) The crystal/melt partitioning of V during mantle melting as a function of oxygen fugacity compared with some other elements (Al, P, Ca, Sc, Ti, Cr, Fe, Ga, Y, Zr and Nb). *J. Petrol.* **50**, 1765–1794.
McKenzie D. and O'Nions R. K. (1995) The source regions of ocean island basalts. *J. Petrol.* **36**, 133–159.
Menzies M. A. and Wass S. Y. (1983) CO_2- and LREE-rich mantle below eastern Australia: a REE and isotopic study of alkaline magmas and apatite-rich mantle xenolith from the Southern Highlands Province, Australia. *Earth Planet. Sci. Lett.* **65**, 287–302.
Moynier F., Yin Q-Z. and Schauble E. (2011) Isotopic evidence of Cr partitioning into Earth's core. *Science* **311**, 1417–1420.
Navon O. and Stolper E. (1987) Geochemical consequences of melt percolation: the upper mantle as a chromatographic column. *J. Geol.* **95**, 285–307.
Nelson D. R., Chivas A. R., Chappell B. W. and McCulloch M. T. (1988) Geochemical and isotopic systematics in carbonatites and implications for the evolution of ocean-island sources. *Geochim. Cosmochim. Acta* **52**, 1–17.

O'Neill H. S. C. and Berry A. J. (2021) The oxidation state of chromium in basaltic silicate melts. *Geochim. Cosmochim. Acta* **306**, 304–320.

Palme H. and O'Neill H. S. C. (2014) Cosmochemical estimates of mantle composition. *Treatise Geochem. 2nd Ed.* **3**, 1–37.

Pogge von Strandmann P. A. E., Elliott T., Marschall H. R., Coath C., Lai Y. J., Jeffcoate A. B. and Ionov D. A. (2011) Variations of Li and Mg isotope ratios in bulk chondrites and mantle xenoliths. *Geochim. Cosmochim. Acta* **75**, 5247–5268.

Preβ S., Witt G., Seck H. A., Ionov D. and Kovalenko V. I. (1986) Spinel peridotite xenoliths from the Tariat Depression, Mongolia. I: Major element chemistry and mineralogy of a primitive mantle xenolith suite. *Geochim. Cosmochim. Acta* **50**, 2587–2599.

Prytulak J., Nielsen S. G., Ionov D. A., Halliday A. N., Harvey J., Kelley K. A., Niu Y. L., Peate D. W., Shimizu K. and Sims K. W. W. (2013) The stable vanadium isotope composition of the mantle and mafic lavas. *Earth Planet. Sci. Lett.* **365**, 177–189.

Reid A. M., Donaldson C. H., Brown R. W., Ridley W. I. and Dawson B. (1975) Mineral chemistry of peridotite xenoliths from the Lashaine volcano, Tanzania. *Phys. Chem. Earth* **9**, 525–543.

Rhodes J. M. and Dawson J. B. (1975) Major and trace element chemistry of peridotite inclusions from the Lashaine volcano, Tanzania. *Phys. Chem. Earth* **9**, 545–557.

Richter F. M., Dauphas N. and Teng F. Z. (2009) Non-traditional fractionation of non-traditional isotopes: Evaporation, chemical diffusion and Soret diffusion. *Chem. Geol.* **258**, 92–103.

Roeder P. L. and Reynolds I. (1991) Crystallization of chromite and chromium solubility in basaltic melts. *J. Petrol.* **32**, 909–934.

Rudnick R. L., McDonough W. F. and Chappell B. W. (1993) Carbonatite metasomatism in the northern Tanzanian mantle: petrographic and geochemical characteristics. *Earth Planet. Sci. Lett.* **114**, 463–475.

Santos J. F., Scha U. and Girardeau J. (2002) Genesis of pyroxenite-rich peridotite at cabo ortegal (NW Spain): Geochemical and Pb – Sr – Nd Isotope Data. *J. Petrol.* **43**, 17–43.

Saunders N. J., Barling J., Harvey J. and Halliday A. N. (2020) Heterogeneous nickel isotopic compositions in the terrestrial mantle – Part 1: Ultramafic lithologies. *Geochim. Cosmochim. Acta* **285**, 129–149.

Schauble E. (2004) Applying stable isotope fractionation theory to new systems. *Rev. Mineral. Geochemistry* **55**, 65.

Schoenberg R., Merdian A., Holmden C., Kleinhanns I . C., Haβler K., Wille M. and Reitter E. (2016) The stable Cr isotopic compositions of chondrites and silicate planetary reservoirs. *Geochim. Cosmochim. Acta* **183**, 14–30.

Schoenberg R., Zink S., Staubwasser M. and von Blanckenburg F. (2008) The stable Cr isotope inventory of solid Earth reservoirs determined by double spike MC-ICP-MS. *Chem. Geol.* **249**, 294–306.

Schreiber H. D. and Haskin L. A. (1976) Chromium in basalts: Experimental determination of redox states and partitioning among synthetic silicate phases. *Proc. Lunar Planet. Sci. Conf.* **7**, 1221–1259.

Shaw D. M. (1970) Trace element fractionation during anatexis. *Geochim. Cosmochim. Acta* **34**, 237–243.

Shen J., Qin L., Fang Z., Zhang Y., Liu J., Liu W., Wang F., Xiao Y., Yu H. and Wei S. (2018) High-temperature inter-mineral Cr isotope fractionation: A comparison of ionic model predictions and experimental investigations of mantle xenoliths from the North China Craton. *Earth Planet. Sci. Lett.* **499**, 278–290.

Shen J., Xia J., Qin L., Carlson R. W., Huang S., Helz R. T. and Mock T. D. (2020) Stable chromium isotope fractionation during magmatic differentiation: Insights from Hawaiian basalts and implications for planetary redox conditions. *Geochim. Cosmochim. Acta* **278**, 289–304.

Siebert J., Corgne A. and Ryerson F. J. (2011) Systematics of metal – silicate partitioning for many siderophile elements applied to Earth's core formation. *Geochim. Cosmochim. Acta* **75**, 1451–1489.

Snow J. E. and Dick H. J. B. (1995) Pervasive magnesium loss by marine weathering of peridotite. *Geochim. Cosmochim. Acta* **59**, 4219–4235.

Sossi P. A., Moynier F. and Van Zuilen K. (2018) Volatile loss following cooling and accretion of the Moon revealed by chromium isotopes. *Proc. Natl. Acad. Sci.* **115**, 10920–10925.

Sossi P. A., O'Neill H. St. and C (2017) The effect of bonding environment on iron isotope fractionation between minerals at high temperature. *Geochim. Cosmochim. Acta* **196**, 121–143.

Streckeisen A. (1976) To each plutonic rock its proper name. *Earth Sci. Rev.* **12**, 1–33.

Sun S.-s. and McDonough W. F. (1989) Chemical and isotopic systematics of oceanic basalts: implications for mantle composition and processes. In *Magmatism in the Ocean Basins* (eds. A. D. Saunders and M. J. Norry). Geological Society Special Publication, pp. 313–345.

Sweeney R. J. (1994) Carbonatite melt compositions in the Earth's mantle. *Earth Planet. Sci. Lett.* **128**, 259–270.

Tuller-Ross B., Marty B., Chen H., Kelley K. A., Lee H. and Wang K. (2019) Potassium isotope systematics of oceanic basalts. *Geochim. Cosmochim. Acta* **259**, 144–154.

Wade J. and Wood B. J. (2005) Core formation and the oxidation state of the Earth. *Earth Planet. Sci. Lett.* **236**, 78–95.

Wagner L. J., Kleinhanns I. C., Weber N., Babechuk M. G., Hofmann A. and Schoenberg R. (2021) Coupled stable chromium and iron isotopic fractionation tracing magmatic mineral crystallization in Archean komatiite-tholeiite suites. *Chem. Geol.* **576** 120121.

Walter M. J. (1998) Melting of garnet peridotite and the origin of komatiite and depleted lithosphere. *J. Petrol.* **39**, 29–60.

Wang X., Amet Q., Fitoussi C. and Bourdon B. (2018) Tin isotope fractionation during magmatic processes and the isotope composition of the bulk silicate Earth. *Geochim. Cosmochim. Acta* **228**, 320–335.

Wang Z. Z., Liu S. A., Liu J., Huang J., Xiao Y., Chu Z. Y., Zhao X. M. and Tang L. (2017) Zinc isotope fractionation during mantle melting and constraints on the Zn isotope composition of Earth's upper mantle. *Geochim. Cosmochim. Acta* **198**, 151–167.

Weyer S. and Ionov D. A. (2007) Partial melting and melt percolation in the mantle: The message from Fe isotopes. *Earth Planet. Sci. Lett.* **259**, 119–133.

Williams H. M., Peslier A. H., Mccammon C. and Halliday A. N. (2005) Systematic iron isotope variations in mantle rocks and minerals: The effects of partial melting and oxygen fugacity. *Earth Planet. Sci. Lett.* **235**, 435–452.

Wood B. J., Wade J. and Kilburn M. R. (2008) Core formation and the oxidation state of the Earth: Additional constraints from Nb, V and Cr partitioning. *Geochim. Cosmochim. Acta* **72**, 1415–1426.

Woodland A. B., Kornprobst J. and Tabit A. (2006) Ferric iron in orogenic lherzolite massifs and controls of oxygen fugacity in the upper mantle. *Lithos* **89**, 222–241.

Xia J., Qin L., Shen J., Carlson R. W. and Ionov D. A. (2017) Chromium isotope heterogeneity in the mantle. *Earth Planet. Sci. Lett.* **464**, 103–115.

Yaxley G. M., Crawford A. J. and Green D. H. (1991) Evidence for carbonatite metasomatism in spinel peridotite xenoliths from western Victoria, Australia. *Earth Planet. Sci. Lett.* **107**, 305–317.

Yaxley G. M., Green D. H. and Kamenetsky V. (1998) Carbonatite metasomatism in the Southeastern Australian Lithosphere. *J. Petrol.* **39**, 1917–1930.

Zhu K., Sossi P. A., Siebert J. and Moynier F. (2019) Tracking the volatile and magmatic history of Vesta from chromium stable isotope variations in eucrite and diogenite meteorites. *Geochim. Cosmochim. Acta* **266**, 598–610.

Associate Editor: Mathieu Roskosz